Experimental study on two-phase flow pattern in inclined straight and helical coil tubes using wire mesh sensor: air-water test at atmospheric pressure

Byeongil You^a, Yujeong Ko^a, Hyunkjae Ko^a, Hyoung Kyu Cho^a*,

^a Department of Nuclear Engineering, Seoul National Univ., 1 Gwanak-ro, Gwanak-gu, Seoul 08826 *Corresponding author: chohk@snu.ac.kr

*Keywords: Helical coil steam generator (HCSG), flow pattern, WMS, centrifugal force

1. Introduction

Among global efforts to achieve net-zero and secure energy security, interest in small modular reactors (SMRs) that can complement the limitations of existing large-scale nuclear power plants is rapidly increasing. For SMRs, maintaining compactness is important. For this reason, many SMRs adopt steam generators made of helically coiled tubes (HCTs) instead of steam generators made of U-tubes, since HCTs can be manufactured more densely for the same heat transfer area.

However, the flow patterns in HCTs can be influenced by the effects of centrifugal force and secondary flow. Flow patterns significantly affect the thermal-hydraulic characteristics, such as heat transfer coefficient and pressure drop. Therefore, defining the flow regime is important to comprehend the specific characteristics of two-phase flow. Flow regime research was conducted for various tube geometries. For straight tubes, Barnea flow regime map is widely used in all range of inclination, which has been mechanistically established through experiments [1]. For HCTs, many previous studies used the straight tube regime map, which has the same inclination angles as HCT's helix angle as the reference regime map [2, 3]. However, discrepancies appeared in the transition area depending on the inner diameter of the tube, the coil diameter, helix angle and etc.

In this study, air-water flow visualization experiments for HCT in atmospheric pressure conditions were performed as a preliminary test to establish the measurement method. To isolate the effects of centrifugal force on the flow pattern, the results from HCT and a straight tube with the same inclination angle as the helix angle of HCT were compared.

2. Experimental apparatus and methods

2.1 Experimental setup

The air-water two-phase flow visualization test loop is shown in **Fig.1**. Experiments were conducted at room temperature and atmospheric pressure. The Test sections consist of an inclined tube and a helically coiled tube (HCT), as illustrated in **Figs. 2** and **3**. The inclination angle of the inclined tube was selected to match the helix angle of the HCT.

At the inlet of the test sections, air and water were injected separately, and then mixed within a porous wall of 50 to $100 \mu m$ holes. At the outlet of the test section,

wire-mesh sensors (WMSs) were installed, ensuring straight length of 70 L/d in the inclined tube and 304 L/d in the HCT, respectively. Downstream of the WMSs, both test sections were connected to a straight pipe to minimize downstream influence.

The flow rates of water were controlled using a pump inverter and a ball valve, and those of air were controlled using a regulator and rotameters. The air and water flow conditions are summarized in **Table 1**.

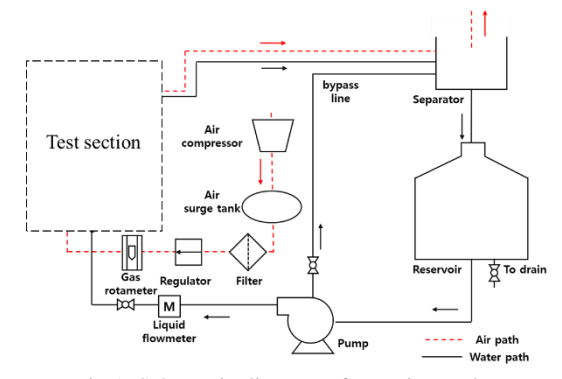


Fig 1. Schematic diagram of experimental setup

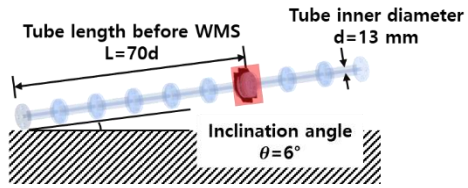


Fig. 2. Geometry information of inclined tube

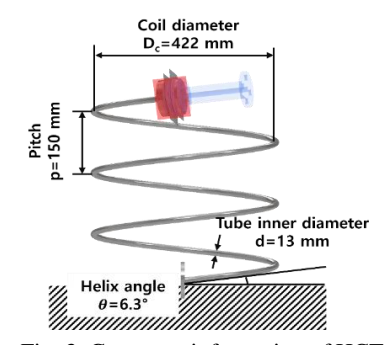


Fig. 3. Geometry information of HCT

Table 1. Experimental condition	
Water superficial velocity (m/s)	0.42-1.67
Air superficial velocity (m/s)	0.01-2.51

2.3 Wire-mesh sensor (WMS)

Wire-mesh sensors (WMSs) were utilizing for measuring the cross-sectional void fraction and phase distribution. The WMSs consist of two electrode planes arranged perpendicular to each other, each plane having metal electrodes spaced equally apart as shown in **Fig. 4** [4]. One plane acts as a transmitter, and the other plane acts as a receiver. The local void fraction is calculated by using the difference in conductivity between the fluids.

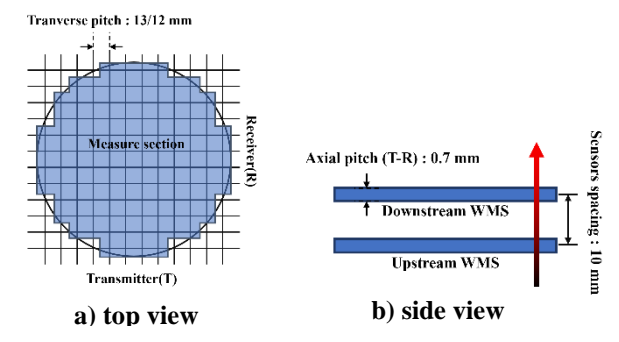


Fig. 4. Schematic diagrams of WMS

2.4 Post-processing method

The post-processing was performed to reconstruct the cross-sectional flow pattern information using raw data from WMSs. The entire process is summarized in Fig. 5. First, in order to calculate spacious or temporal averaged void fraction value, the data must be converted to void fraction. To convert conductivity data into the void fraction data, raw data were calibrated with liquid-only data. Considering the overshooting phenomenon of conductivity at the air-water interface, the Maxwell nocut relation was adopted as the conversion method, as shown in Eq. (1).

$$\alpha^* = \begin{cases} 0 & (\alpha^* < 0) \\ \frac{1 - \frac{\sigma^*}{\sigma_{lo}^*}}{1 + \frac{\sigma^*}{2\sigma_{lo}^*}} & (0 \le \alpha^* < 1) \\ 1 & (1 \le \alpha^*) \end{cases}$$
 (1)

Afterwards, several bubble properties were calculated: axial mean velocity of air, bubble volume, and cross-sectional area. The air-mean axial phase velocity was calculated by measuring the time it takes for the same bubble to pass from the upstream WMS to the downstream WMS. Lastly, the data reconstruction process was performed to extract the images and videos for analysis, including cross-sectional average void fraction area and 3-D reconstructed flow regime.

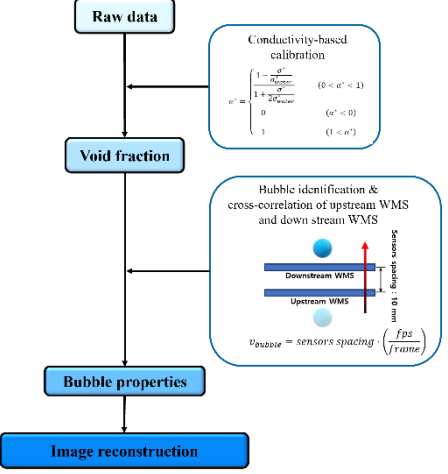


Fig. 5. Post-processing method using WMS data

3. Results of flow pattern comparison for the inclined tube and HCT

3.1. time-averaged plane void fraction

In HCT, buoyancy acts in the opposite direction of the resultant force between gravitational force and centrifugal force. The force balance and position in the cross-section of HCT are described in **Fig. 6**. In this section, the time-averaged cross-sectional void fraction distributions were compared between the inclined tube and HCT to confirm effect centrifugal force on phase distribution, from low to high water flow rate with same air flow rate ($j_q = 0.01 \ m/s$), as shown in **Fig.7**.

At low water flow rates and low air flow rates (**Fig.7-(a**)), gravitational force is dominant, causing bubbles to concentrate at the top of the tube cross-section in both the inclined tube and the HCT. Therefore, the time-averaged cross-sectional void fraction distributions of the HCT were similar to those of the inclined tube.

At high water flow rates (**Fig.7-(c**)), due to the stronger centrifugal force effect which is proportional to square of phase velocity, the buoyancy in the HCT acted in the top-inner direction [5]. Therefore, bubbles in the HCT were concentrated between the top and inner regions while the bubbles in the inclined tube remained at the top region at high flow rates.

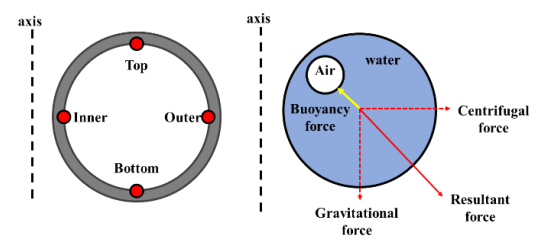


Fig 6. Nomenclature of cross-sectional position and force balance of air-water flow inside of the HCT

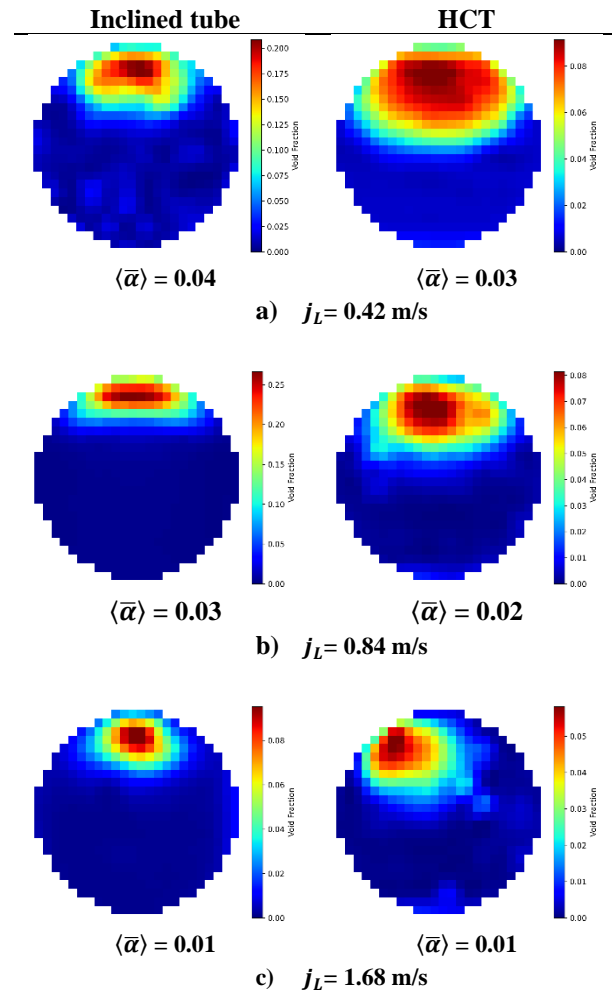


Fig. 7. Time-averaged cross-sectional void fraction distribution in the inclined tube and $HCT(j_g = 0.01 \ m/s)$ according to changes in j_L

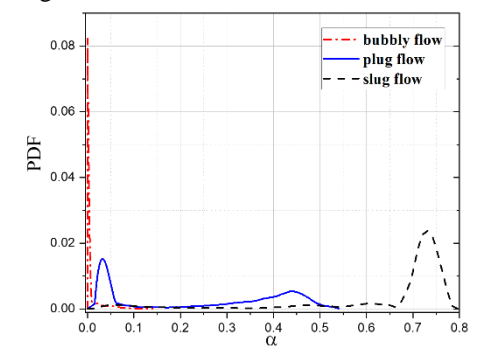
3.2. flow regime transition

The flow regime in the inclined tube and HCT under the given conditions were determined. Determining the flow regime criteria was based on probability density function (PDF) [2] and the shapes of gas phase in both inclined tube and HCT. The PDF is a statistical representation of some properties (void fraction for this case) that indicates the likelihood of observing specific values and thus reflects the dominant flow characteristics.

For bubbly flow, as can be seen in the **Fig. 8**, the PDF of void fraction peaks at void fraction lower than 0.01, and bubbles are dispersed and small. Plug flow and slug flow have two peak points, which indicates that gasplug/slug and liquid-plug/slug pass through tube cross-section alternately. Slug flow has a larger peak at higher void fraction ($\alpha > 0.5$), contrary to plug flow which has a smaller peack at lower void fraction because the gasslug is longer than the liquid slug.

Based on the above characteristics, the flow regime map of the inclined tube and HCT were obtained. In **Fig. 9**,

both the bubbly-plug transition and plug-slug transition occur in the lower j_g for HCT than the inclined tube. This is because centrifugal force causes water to accumulate on the outside and air on the inside, promoting bubble coalescence.



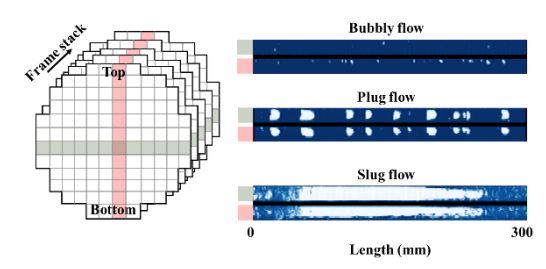


Fig. 8. Examples of void fraction distribution and the shapes of gas phase with length scale inside of tube

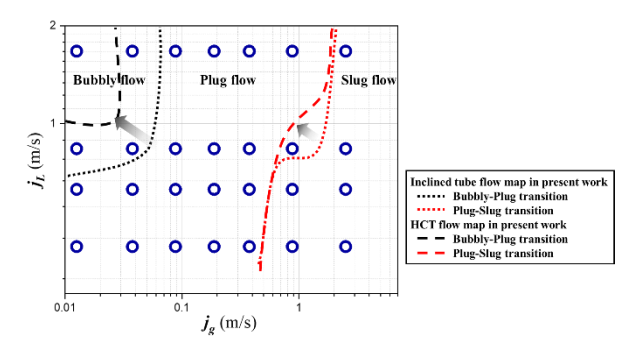
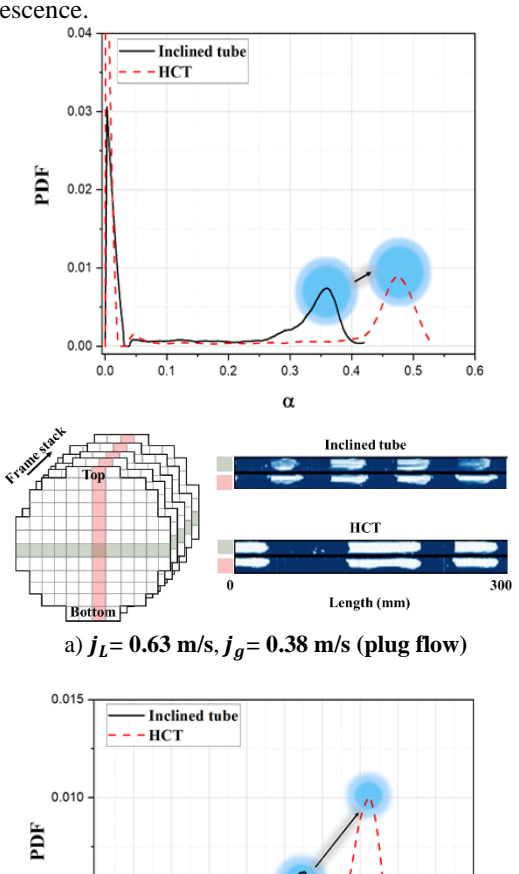


Fig. 9. Comparison of flow regime map between the inclined tube and HTC for given conditions

To further investigate the differences in flow pattern characteristics due to the centrifugal force effect, PDFs were compared between the inclined tube and HCT under the same flow rate conditions, as shown in Fig. 10. In both slug and plug flow regimes, the void fraction exhibited a wider range with higher peaks in the HCT. This is attributed to the centrifugal force in the HCT, which induces greater interfacial turbulence compared to the inclined tubes, where only gravitational force acts. Furthermore, the gas-phase lengths of both slug and plug flow were longer in HCT, as the combined effects of the

centrifugal force and secondary flow promote bubble coalescence.



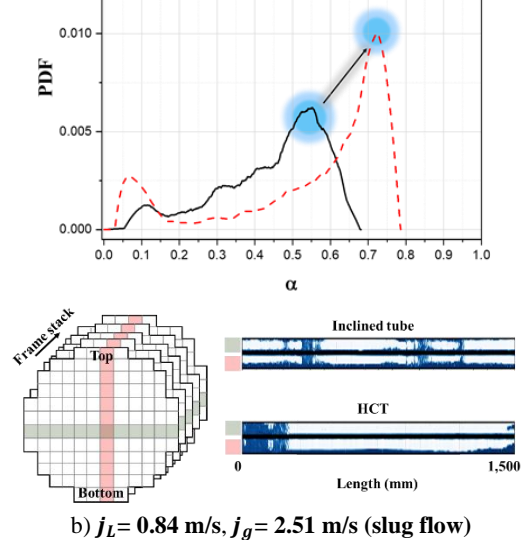


Fig 10. Comparison of void fraction distribution and shapes of gas phase with length scale between inclined tube and HCT

To quantify the centrifugal force effect in HCT, the angle between the bubble centroid and the tube crosssection centroid, θ_h , was calculated and compared to the liquid-based Froude number Fr_L . θ_b is calculated from the time-averaged cross-sectional void fraction obtained in Fig. 7 by capturing the area with a high void fraction and calculating the angle formed with the center of the cross-section as shown in Fig. 11. The liquid-based Froud number was calculated using Eq. (2). Since the phase velocity of the liquid cannot be obtained using WMS, it is calculated using the time-cross-sectionalaveraged void fraction ($\langle \overline{\alpha} \rangle$), as shown in Eq. (3).

The cross-sectional bubble position with the θ_h along the Fr_L and the time-averaged cross-sectional void fraction image are shown in Fig. 12. For the inclined tube, θ_b was from -13° to 13°. This range can be interpreted as an uninfluential region without physical significance, so this part is shown as the gray region in Fig. 12. When Fr_L is less than 1.0, gravitational force is dominant. Therefore, the bubble concentrated on the top side ($\theta_b \cong$ $\mathbf{0}^{\circ}$). When Fr_L exceeds 1.0, centrifugal force becomes larger than gravitational force, causing the direction of buoyancy to shift from the top toward the inner side. Therefore, θ_b remains over 13° for most cases as the $\mathbf{Fr_L}$ increases. In other words, when $\mathbf{Fr_L}$ is greater than 1.0, centrifugal force dominates over gravitational force in HCTs, causing the liquid phase to be pushed outward and the gas phase to be pushed inward, resulting in differences in flow patterns compared to straight tubes.

$$Fr_{L} = \frac{u_{L}^{2}}{gD_{c}}$$

$$u_{L} = \frac{j_{L}}{1 - \langle \overline{a} \rangle}$$
(2)

$$u_L = \frac{j_L}{1 - \langle \overline{\alpha} \rangle} \tag{3}$$

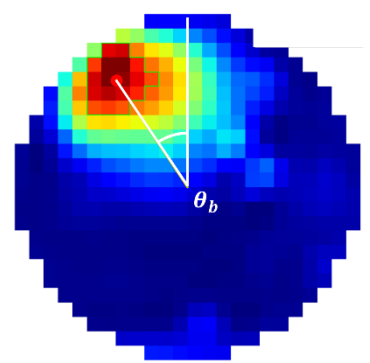


Fig. 11. Schematic diagram of θ_b

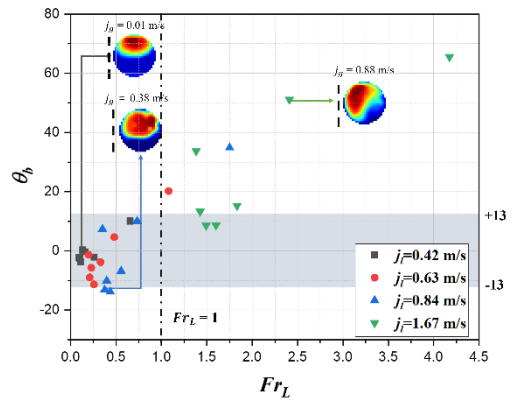


Fig. 12. Relationship between bubble and tube cross-section according to Froude number

4. Conclusion

In this study, the effects of centrifugal and secondary flow forces in HCTs were examined by comparing flow patterns in air-water visualization experiments of the HCT and the inclined tube. WMSs were applied to measure cross-sectional void fraction and reconstructed into 3D flow pattern images with post-processing. As a result, bubbly flow to slug flow was observed in both the inclined tube and HCT. Comparison of the flow pattern transition between the inclined tube and HCT shows that earlier transition than the inclined tube. The peak point of the PDF distribution shifted to the right and slug length in HCT is longer than in inclined tube because of bubble coalescence induced by the resultant force.

The centrifugal force effect of HCT was quantified by comparing the bubble angle from the center of the tube with the liquid Froude number. Consequently, it was confirmed that when the Froude number exceeds 1.0, the bubble shifted towards the top-inner side, and the effects of centrifugal force became apparent. Future work will be extended to broaden flow regions, including the annular flow regime.

AKNOWLEDGEMENT

This work was supported by the Innovative Small Modular Reactor Development Agency grant funded by the Korea Government (MSIT) (No. RS-2024-00408520).

REFERENCES

- [1] Barnea et al., "A unified model for predicting flow-pattern transitions for the whole range of pipe inclination", International Journal of Multiphase Flow Vol 13, No. 1, pp. 1-12, 1987
- [2] Li Liu et al., "Recognition of Gas-Liquid Flow Regimes in Helically Coiled Tube Using Wire-Mesh Sensor and KNN Algorithm," International Journal of Multiphase Flow 154 (September 2022): 104144,
- [3] Breitensomer et al., "Machine learning based flow regime recognition in helically coiled tubes using X-ray radiography", International Journal of Multiphase Flow 161 (2023) 104382
- [4] H.-M. Prasser et al., "A new electrode-mesh tomograph for gas-liquid flows", Flow Measurement and Instrumentation 9 (1988) 111-119
- [5] Li Liu et al., "Flow pattern transition and void fraction prediction of gas-liquid flow in helically coiled tubes", Chemical Engineering Science 258 (2022) 117751